RADIATION RESEARCH 82, 27–44 (1980)

Secondary Electron Emission from Ionization of Water Vapor by 0.3- to 2.0-MeV He^+ and He^{2+} Ions[1]

L. H. TOBUREN, W. E. WILSON, AND R. J. POPOWICH

Pacific Northwest Laboratory, Richland, Washington 99352, and U. S. Department of Energy, Oakland, California 94612

TOBUREN, L. H., WILSON, W. E., AND POPOWICH, R. J. Secondary Electron Emission from Ionization of Water Vapor by 0.3- to 2.0-MeV He^+ and He^{2+} Ions. *Radiat. Res.* **82,** 27–44 (1980).

Yields of secondary electrons (δ rays), differential in ejected electron energy and emission angle, are reported for 0.075 to 0.5 MeV/amu helium ions, both singly and doubly charged (α particles) arising from single collisions with water molecules in vapor phase. Results are compared with similar data reported previously for protons with the same velocity. We found that the bound electron of the He^+ ion effectively screens the nuclear charge for collisions at large impact distances, thereby suppressing the yield of low-energy secondaries while contributing directly to the yield of high-energy secondaries. This results in a secondary electron spectrum of higher mean energy and lower total yield for He^+ than the bare He^{2+} produces. Comparison of the yields for He^{2+} with similar data for protons indicates deviations from Z^2 scaling which occur primarily for secondary electrons ejected at small angles and, hence, close to the path of the primary ion and for electron velocities similar to the ion velocity. These results imply that the detailed structure of helium ion tracks is somewhat different from what would be predicted from a simple Z^2 scaling of proton track structure.

INTRODUCTION

For charged particles having energies greater than about 100 keV/amu, the principal means of energy loss is ionization of the stopping media (*1, 2*). The radiochemical and biological effectiveness of fast charged particles is therefore closely related to the energy and spatial distributions of secondary electrons generated along the path of the passing ion. An extensive literature has been generated which focuses on the production of secondary electrons by bare charged particles such as protons (*3–13*) and electrons (*3, 14–20*). Little is known, however, about the yields of secondaries for incident charged particles which themselves carry bound electrons (*21–25*). These bound electrons provide electrostatic screening of the nuclear charge of the projectile and contribute to the electron distribution released to the stopping media as they become stripped from the incident ion. We recently published extensive measurement of the ionization of argon by helium ions (*24*); the measurements reported here concentrate on ionization of the radiologically important water molecule. The energy range of the incident helium ions included in these measurements is from 0.3 (0.075 MeV/amu) to 2.0 MeV (0.5 MeV/amu). Comparison of results of this measurement with previous data for protons of similar

[1] Based on work performed under United States Department of Energy Contract EY-76-C-06-1830.

0033-7587/80/040027-18$02.00/0

velocity provides detailed information regarding Z^2 scaling and the effects of screening by the ionic electrons on ionization and energy loss cross sections.

EXPERIMENTAL TECHNIQUE AND RESULTS

Ionization cross sections, differential in ejected electron energy and emission angle, were measured for He^+ and He^{2+} (α particle) ion energies of 0.2, 0.3, 0.4, and 0.5 MeV/amu. In addition, He^+ cross sections were measured at 0.075 MeV/amu (available beam intensity was inadequate for measurements with He^{2+} at 0.075 MeV/amu). Electron energy spectra were recorded at angles from 10 to 125° with respect to the forward direction of the charged particle beam. Absolute cross sections, differential in ejected electron energy and emission angle, were derived directly from knowledge of the experimental parameters. Integration of these double differential cross sections with regard to electron energy and/or emission angle provide single differential and total cross sections for ionization.

The experimental technique has been described in previous publications concerning ionization by protons (*5–8, 13*), so only a brief description will be provided here. The He^+ beam was produced by an r-f ion source, accelerated by a Van de Graaff accelerator, momentum analyzed, and transported several meters before being magnetically deflected into the collision chamber. The inflection magnet preceding the collision chamber provided charge state purity of the ion beam. For measurements requiring a He^{2+} beam, a small amount of gas was leaked into the beam transport region between the analyzing and inflection magnets, thus forming He^{2+} by stripping the incident He^+ beam. This was necessary as the r-f ion source produces too little He^{2+} to provide a beam via direct extraction. The second magnet then was used to select the He^{2+} component of the beam and deflect it into the collision chamber. Using this method of charge state preparation, accurate relative cross sections could be obtained for He^+ and He^{2+} since minimal changes in operating parameters were required to change from one charge state to the other.

After charge state selection by the inflection magnet, the ion beam was collimated, passed through a differentially pumped collision region, and collected in a shielded Faraday cup. Electrons, released in ion-molecule collisions, left the collison region through a slit in the differentially pumped gas cell, were energy analyzed by a cylindrical mirror electrostatic analyzer, and were detected by a continuous channel electron multiplier. Absolute cross sections were obtained from the experimental parameters such as target gas density, solid angle subtended by the analyzer, detection efficiency, etc. A complete description of the data reduction leading to absolute cross sections and the uncertainties contributed by various parameters is provided in Ref. (*13*).

An example of the cross section surfaces generated by these measurements is shown in Fig. 1, where cross sections for ionization of water vapor by 0.3 MeV/amu He^+ and He^{2+} ions are shown. The principal difference between the cross section surfaces generated by these two ions is the appearance of a broad ridge in the He^+ spectra occurring at about 160 eV with maximum intensity at small emission angles. This contribution is due to electrons which are stripped from the incident He^+ ions. The energy of 160 eV at which the peak maximizes corresponds

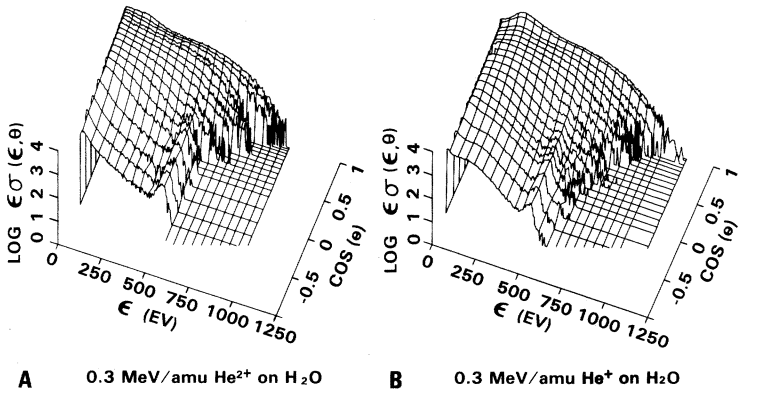

FIG. 1. Double differential cross sections for ionization of water vapor by 0.3 MeV/amu helium ions; He^{2+} (α particle) impact and He^{+} impact; $\epsilon\sigma(\epsilon,\theta)$ in units of 10^{-20} eVcm^2.

to the energy of an electron released with zero kinetic energy in the rest frame of the He^{+} ion. Features common to the spectra for both He^{+} and He^{2+} ions are maxima in the spectra at each angle for emission of low-energy electrons and, for a given electron energy, a maximum in the emission cross sections for small emission angles.

The uncertainty in the absolute value of the measured cross sections is estimated as $\pm 20\%$ derived from estimated uncertainties in the various experimental parameters such as target density, solid angle, detection efficiency, etc. Uncertainties are larger for electron energies less than about 15 eV due to effects of residual electric and magnetic fields and for the highest electron energies where statistical uncertainties become significant. For comparison between the He^{+} and He^{2+} cross sections and for comparison of the helium ion results with previous proton measurements of this laboratory, the relative uncertainties are expected to be $\pm 10\%$. This reduced uncertainty occurs because the same experimental apparatus was used (i.e., same geometry, gas pressure, and detection efficiencies) with only minor changes due to acceleration of the different ion beams.

DOUBLE DIFFERENTIAL CROSS SECTIONS

A comparison of the ejected electron energy spectra for the highest and lowest energy He^{+} and He^{2+} ions is shown in Fig. 2 for selected electron emission angles. Similar velocity proton data, multiplied by a factor of 4 to account for Z^2 scaling, are also shown for 0.5 MeV/amu ion impact. Corresponding proton results are not available for the lowest helium ion energies studied. The comparison of He^{+} and He^{2+} data in Fig. 2 clearly illustrates the effect of screening the nuclear charge of He^{+} by its bound electron. For collisions involving small energy transfer, ejection of low-energy electrons, the mean distance of closest approach is large and the nuclear charge of the helium ion is effectively screened. The impact parameter associated with large energy transfer, energy transfer greater than a few hundred electron volts for the ion energies considered here, is sufficiently small that the bound He^{+} electron provides little screening, and the ionization cross sections

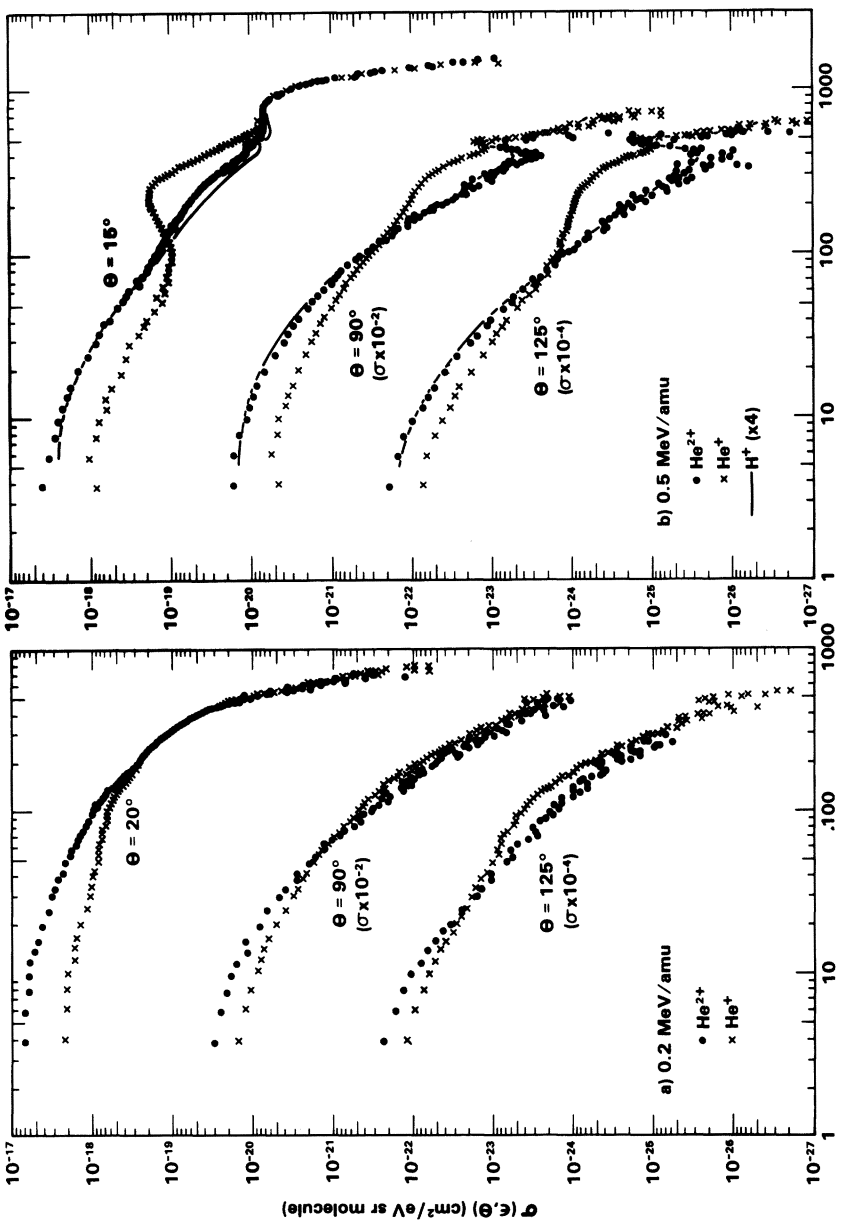

FIG. 2. Ejected electron energy spectra for ionization of water vapor by equal velocity He^+, He^{2+}, and H^+ for selected electron emission angles. The proton data of Toburen and Wilson (7) are multiplied by 4 for Z^2 scaling.

are equal for He^+ and He^{2+} ions. The energy transfer at which the differential cross sections for He^+ and He^{2+} ions become equal is observed to depend on the projectile energy and the angle at which the electron is ejected. Such a dependence is expected since the minimum momentum transfer required for a given energy transfer is a function of the ion energy and collision kinematics (*26*).

In addition to the importance of screening illustrated in Fig. 2, these data also show the significance of the bound electron of the He^+ as a contributor to the ejected electron spectra. For fast projectiles, the probability of stripping the electron from the incident ion is high, and these electrons are observed as a prominent broad peak in the electron spectrum. This contribution is the dominant structure in the 0.5 MeV/amu He^+ spectra of Fig. 2, whereas the 0.2 MeV/amu results show only a small indication of projectile stripping. Since these electrons are stripped from the He^+ ion with essentially zero energy in the rest frame of the ion, the major contribution in the laboratory frame is expected for electron energies given by $\epsilon = \frac{1}{2} m_e v_i^2$, where m_e is the electron mass and v_i the ion velocity. The width of the peak depends on the initial velocity distribution of the bound electrons and also on transformation of the ejected electron distribution from the rest frame of the incident ion to the laboratory reference frame. The width at the base of this peak can be estimated to first order by $4(E_B E_i)^{1/2}$, where E_B is the binding energy of the He^+ electron and E_i is the mean ejection energy as observed in the laboratory (*23*). This calculation predicts a base width of approximately 465 eV for electrons stripped from 0.5 MeV/amu He^+ ions, which is in good agreement with the results shown in Fig. 2b. Although no evidence of projectile stripping is observed for electron emission into small angles for low energy He^+ impact, there is nearly a factor of 2 enhancement of the He^+ cross section over the He^{2+} values for ejection of electrons near 100 eV into large emission angles. The cross section for ionization of target electrons appears to decrease more rapidly with increasing angle than for ionization of the projectile into the same laboratory angle; this results in the small contribution due to electron stripping becoming significant at the large emission angles.

Evidence of a departure from Z^2 scaling between cross sections for protons and equal velocity alpha particles is illustrated by the 0.5 MeV/amu data shown in Fig. 2b. Although excellent agreement between scaled proton and α particle data is observed for large emission angles, differences of the order of 20% are noted at ejected electron energies from approximately 100 to 600 eV in the spectra measured for small angles. These differences occur in the energy and angular region where ionization of the target through the process of charge-transfer-to-the-continuum has been shown to be important (*3, 4*). An implication of this difference is that continuum-charge-transfer is not scaled as Z^2.

This result is in qualitative agreement with recent measurements of Vane *et al.* (*27*) who report that continuum-charge-transfer for bare ions varies as $Z^{2.2}$, and theoretical work which predicts a Z^3 dependence (*28*).

The sharp peak in the emission spectra at about 540 eV results from Auger electron emission following K-shell ionization in the oxygen atom of the water vapor molecule. Within the ion velocity range of these measurements, the K-shell ionization cross section of oxygen is increasing with ion energy (*29*). For this

reason, only a small indication of Auger emission is observed in the electron spectra for the low-energy ions. Because the emphasis of the present investigation was on determination of continuum cross sections encompassing a broad range of ejected electron energies and angles, insufficient counting statistics were obtained to provide a detailed analysis of the Auger structure. Auger electron emission will be discussed only as it relates to interpretation of the electron spectra resulting from direct ionization of the target or projectile.

The angular distribution of ejected electrons can be examined in more detail by plotting the cross sections at selected electron energies for the full range of angles covered by these measurements. Angular distributions for emission of electrons of selected energies are shown in Fig. 3a for 0.075 MeV/amu He^+ ions and in Fig. 3b for 0.2 MeV/amu for He^+ and He^{2+} ions; inadequate He^{2+} beam intensity precluded comparison of He^+ and He^{2+} cross sections at 0.075 MeV/amu. For these low ion velocities, the emission cross sections for He^{2+} exhibit a monotonic decrease with emission angle for all electron energies. The cross sections for He^+ also decrease as the emission angle increases except for the cross sections at intermediate energies which increase again at the largest angles studied. This slight increase at large angles is attributed to the contribution of electrons stripped from the He^+ ions and corresponds to the broad peaks observed in the electron energy spectra of Fig. 2. The general trend of the cross sections to maximize at small emission angles and monotomically decrease with increasing emission angle is similar to previously reported results for ionization of noble gases by slow protons (*9, 11*).

The comparison of He^+ and He^{2+} cross sections in Fig. 3b illustrates the effect

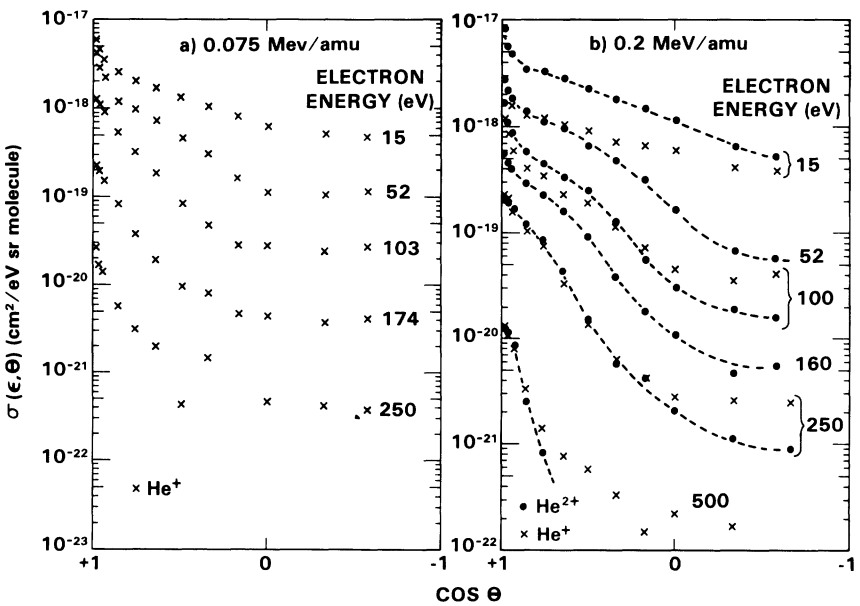

FIG. 3. Angular distributions of electrons of selected energies ejected in the ionization of water vapor by (a) 0.075 MeV/amu He^+ ions, and (b) 0.2 MeV/amu He^+ and He^{2+} ions.

of projectile structure on the angular distribution of electrons ejected in ionizing collisions. For low electron energies, the effect of screening is observed as a decrease in the He^+ cross sections relative to those for He^{2+}. This effect is largest for ejection of electrons into small angles and decreases as the angle increases. The angular distribution of 100-eV electrons ejected in He^+ collisions includes the contribution from electrons stripped from the He^+ ion. This contribution is maximum when the electron and outgoing ion have nearly the same velocity, about 100 eV for the 0.2 MeV/amu ions of Fig. 3b, but influence the spectra over a broad range due to the large width of the stripped electron distribution. For low velocity projectiles, such as illustrated in Fig. 3, the enhancement in the electron yields due to stripping electrons from the projectile is compensated by a decrease in direct ionization due to screening of the He^+ nuclear charge. In the 0.2 MeV/amu case shown in Fig. 3b, the effect of screening is most important for electron ejection into small angles where direct ionization of the target molecule is the dominant contribution; for angles less than about 70°, cross sections for emission of 100-eV electrons are greater for He^{2+} than He^+. At larger angles, the contribution to the cross section from stripped electrons dominates and the He^+ cross sections are largest. At all electron energies shown, the He^+ cross sections are more isotropic than the corresponding He^{2+} values.

The comparison of angular distributions of electrons arising from ionization of water vapor by He^+ and He^{2+} ions is extended to higher ion velocities in Fig. 4, where equal velocity proton results (*7*) multiplied by 4 to account for Z^2 cross section scaling have also been included. As was observed at lower ion velocities,

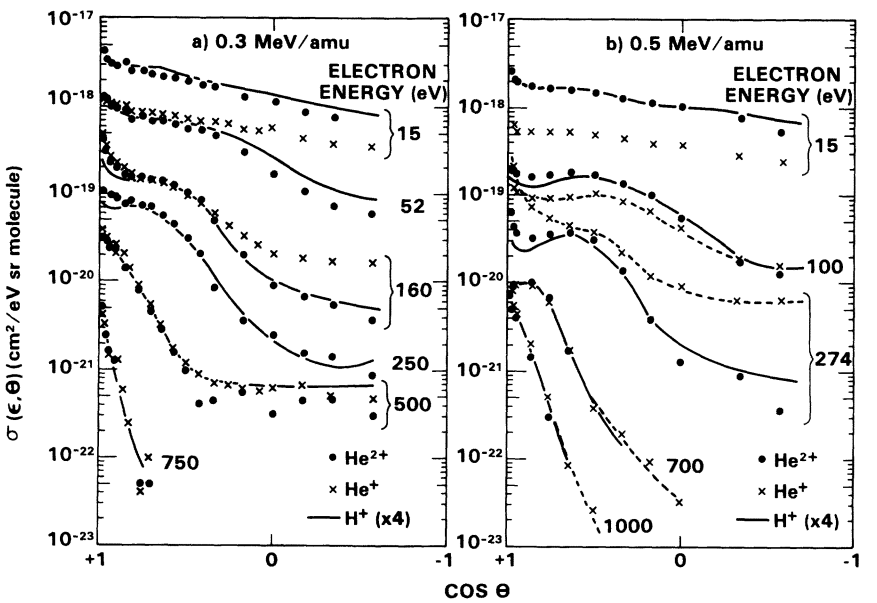

FIG. 4. Angular distributions of electrons of selected energies ejected in ionization of water vapor by (a) 0.3 MeV/amu He^+, He^{2+}, and scaled H^+ ions, and (b) 0.5 MeV/amu He^+, He^{2+}, and scaled H^+ ions. The proton data of Toburen and Wilson (*7*) are multiplied by 4 for Z^2 scaling.

the cross sections are maximum for small emission angles and decrease as the angles increase. There is now, however, evidence of a secondary peak occurring for emission of electrons with energies above about 50 eV. This secondary peak is associated with high-energy collisions in which the interaction approximates the classical charged-particle free-electron collision. This binary encounter peak would be observed as a δ-function distribution in energy and at an emission angle defined only by classical collision kinetics, if the collision were between an ideal fast-charged particle and a free electron. In the real case, the peak is broadened by the effects of the binding energy on the target electrons and at these ion energies by the molecular nature of low energy collisions.

The comparison of He^+ and He^{2+} cross sections at 0.3 and 0.5 MeV/amu in Fig. 4 shows effects of screening and projectile stripping similar to the lower ion energies of Fig. 3. As the ion energy increases, however, the angular distributions of the cross sections for low-energy electron ejection become more similar for the two ions; the effect of screening becomes less angularly dependent. For high-energy ejected electrons, $\epsilon \gtrsim 500$ eV, there is excellent agreement between He^+ and He^{2+} cross sections. The angular distributions for ejection of electrons having velocity similar to the incident ion, 160 and 275 eV for the 0.3 and 0.5 MeV/amu ions, respectively, clearly indicate the increasing importance of electron stripping as the He^+ ion velocity increases. For 0.5-Mev He^+ ions, the cross section for emission of 275-eV electrons at large and small angles is nearly an order of magnitude greater than the corresponding He^{2+} cross sections.

Comparison of electron emission cross sections for He^{2+} interactions with results for equal velocity H^+ impact provides detailed information on the relevant range in energy transfer and the mechanisms responsible for deviations from Z^2 scaling in ionizing collisions. Within the energy range of the present measurements, excellent agreement is observed between He^{2+} and scaled H^+ results with the exception of cross sections for emission of electrons into small angles with velocities near that of the incident ion. As noted before, this is the region of the ejected electron spectrum where continuum-charge-transfer is expected to be important. In the data presented here, the only divergence from Z^2 in ionizing collisions occurs in just those areas where the continuum-charge-transfer mechanism is known to be important and which furthermore has been shown to have a higher Z dependence (*27, 28*).

SINGLE DIFFERENTIAL CROSS SECTIONS

Single differential electron emission cross sections, $\sigma(\epsilon)$, were obtained from our measured double differential cross sections by integration with respect to ejected electron angle. These cross sections are conveniently illustrated by considering the ratio of $\sigma(\epsilon)$ to the corresponding Rutherford cross section. The utility of this representation of the cross sections is that it removes the principal dependence of the cross sections on energy and energy loss of the incident ion which makes possible a convenient display of the spectra on a linear scale. In addition, if the ratio is plotted vs the reciprocal of energy loss, the area under the resulting curve is proportional to the total ionization cross section. This permits a direct evaluation

of the importance of spectral features as contributors to the ionization process. The use of this ratio for analysis of single differential cross sections has been described in detail in previous work on ionization by electrons and protons [see Ref. (*10*) and references therein]. The ratio of measured differential cross section to Rutherford cross section per target electron is defined (*10*) as:

$$Y(E,T) = \frac{T}{4\pi a_0^2 R^2 Z^2} \sum_j (\epsilon + I_j)^2 \sigma_j(\epsilon), \tag{1}$$

where a_0 is the Bohr radius (0.529 Å), R is the hydberg (13.6 eV), Z is the atomic number of the projectile, T is the kinetic energy of an electron traveling at the projectile speed ($T = \frac{1}{2} m_e v_1^2$), I_j is the binding energy on an electron ejected from the j^{th} subshell of the target molecule, and E is the energy loss taken to be the sum of ejected electron kinetic energy ϵ and ionization potential I_j. Since our measurement does not distinguish from which bound state an electron originated, it was assumed for this analysis that all electrons are initially bound with the valence binding energy. This approximation is reasonable, since inner shell ionization cross sections are relatively small within this ion energy range and the outer electrons are bound with energies which differ little compared to the kinetic energy of the ejected electrons. With this approximation, Eq. (1) becomes:

$$Y(E,T) = \frac{T}{4\pi a_0^2 R^2 Z^2} (\epsilon + I)^2 \sigma(\epsilon), \tag{2}$$

where I is the valence binding energy.

Although some detail is lost in performing the integration, comparison of single differential cross sections provides insight into the effects of screening and projectile stripping on energy loss through ionizing collisions. Plots of $Y(E,T)$ vs R/E provide a convenient illustration of the importance of various spectral features on the ionization yield since, as indicated above, equal areas under the curves contribute equally to the total ionization cross section. Plots of $Y(E,T)$ vs R/E are shown in Fig. 5 for (a) 0.2, (b) 0.3, (c) 0.4, and (d) 0.5 MeV/amu He^+ and He^{2+} ionization of water vapor. Proton data are available for comparison at 0.3 and 0.5 MeV/amu, and these are shown in Fig. 5 to illustrate the applicability of Z^2 scaling. Comparison of spectra for He^+ and He^{2+} clearly illustrates the importance of the bound He^+ electron on the ionization process. The He^+ ion is a factor of 2 to 3 less effective in producing low-energy electrons due to the screening of the nuclear charge by the bound electron. As larger values of energy loss are considered, small impact parameters become important, making screening ineffective; and at the high-energy end of the spectra the He^+ and He^{2+} results coincide. The relative contribution to the ejected electron spectra due to electrons stripped from the He^+ ion is also apparent in Fig. 5. For the high-energy ions, the spectra for He^+ are enhanced by contributions from electron stripping, thereby increasing the ratio well over the corresponding values for He^{2+} or H^+. For the highest energy shown, the contribution to the total electron yield arising from ionization of the projectile reaches 20 to 30%. In contrast, the spectrum for the lowest energy shown, 0.2 MeV/amu, shows no evidence of a contribution from electron stripping; at no

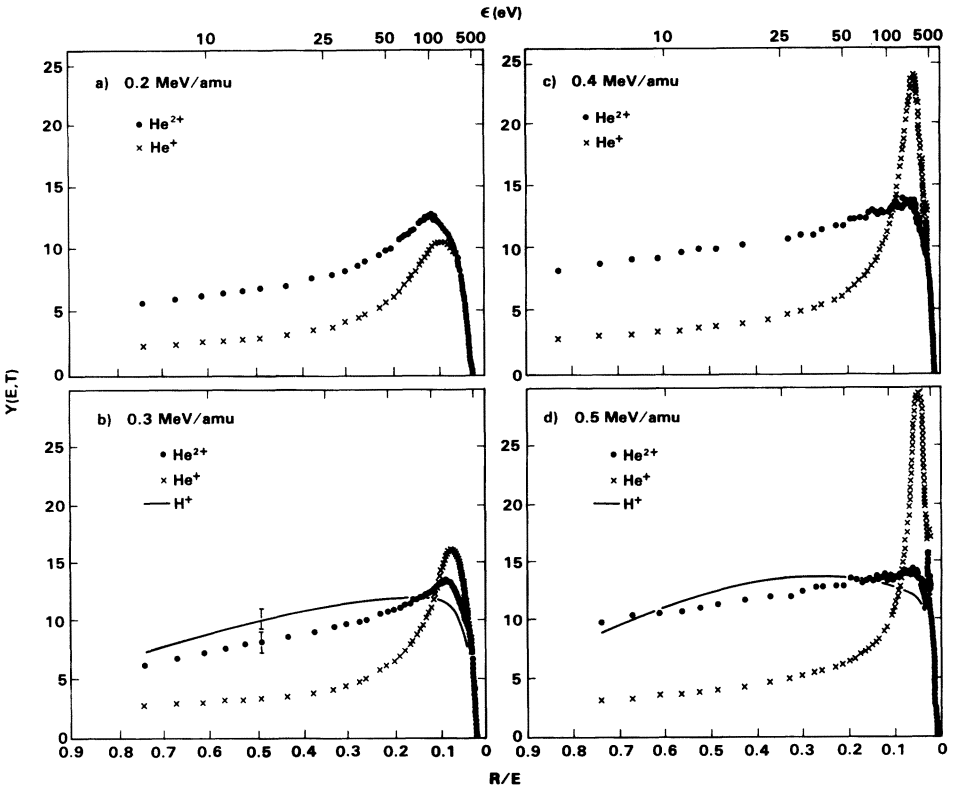

FIG. 5. Ratio of the measured differential cross sections to the corresponding Rutherford cross section per electron for (a) 0.2, (b) 0.3, (c) 0.4, and (d) 0.5 MeV/amu helium ions plotted vs R/E where E is the collisional energy loss, given by the sum of electron kinetic energy and valence binding energy, and R is the hydberg unit of energy (R = 13.6 eV). The proton results for 0.3 and 0.5 MeV/amu are from Toburen and Wilson (*7*).

point is the He^+ spectrum larger than the He^{2+} result. The principal effect of projectile structure on the yield of electrons is that of screening, which reduced the He^+ cross sections for small energy transfer. From the data shown in Fig. 5, it is apparent that the relative number of high-energy electrons ejected in ionizing events is larger for He^+ than He^{2+}, although the total cross section for ionization is greater for He^{2+}. As higher velocity ions are considered, projectile stripping becomes more important and the cross sections for He^+ impact become larger than the cross sections for He^{2+} impact in the spectral regions where electrons are ejected with velocities comparable to the ion velocity. This stripping contribution and the effect of screening by the projectile electron combine to produce electron spectra with a much higher mean energy for He^+ than for the bare He^{2+} ion. The mean energies and total yields will be discussed further in the next section of this paper.

The comparison of equal velocity H^+ and He^{2+} results in Fig. 5 provides further evidence of the applicability of Z^2 scaling in this ion velocity range. Note that in contrast to comparisons of Figs. 2 and 4, these spectra are plotted on a linear

scale. In general, the proton data are in good agreement with the scaled He^{2+} results, although there is a difference in the overall shapes of the spectra. The 0.3 MeV/amu results for protons appear larger than the He^{2+} cross sections in the range of 10 to 50 eV of electron energy. This difference is only slightly outside the expected relative uncertainties in these measurements. The error bars shown in Fig. 5b represent a relative uncertainty of $\pm 10\%$ assigned to these data which were all obtained using the same experimental arrangement. There is somewhat better agreement in this range of 10 to 50 eV for the 0.5 MeV/amu results. Because the disparities are so nearly within the experimental precision, it is not clear that the closer agreement for the higher ion energy is significant. The discrepancies between proton and scaled He^{2+} data for ejected electron energies near $v_e \simeq v_i$ were discussed earlier and attributed to non-Z^2 scaling of ionization through the continuum-charge-transfer process which is important in this energy range.

The influence of projectile structure on the single differential cross sections can also be evaluated by plotting the ratio of He^+ cross sections to the corresponding He^{2+} values as a function of the ejected electron energy. These ratios, shown in Fig. 6 for ion energies from 0.2 to 0.5 MeV/amu, provide a convenient means of assessing the relative importance of the bound electron to the energy loss process. For ejection of low-energy electrons, i.e., small energy loss by the ion, the ratio of cross sections decreases due to screening of the nuclear charge by the He^+-bound electron. For large impact parameters associated with ejection of near zero energy electrons, this ratio should tend toward a value of 0.25, representing a fully screened nuclear charge. For ejection of fast electrons, small impact parameter collisions dominate, making screening ineffective, and the cross section ratio approaches a value of 1. For ejected electron energies in the range from 100 to 400 eV, the ratio goes well over 1 for the high-energy ions due to the large contribution from electrons stripped from the He^+ ion. It is interesting that the centroid

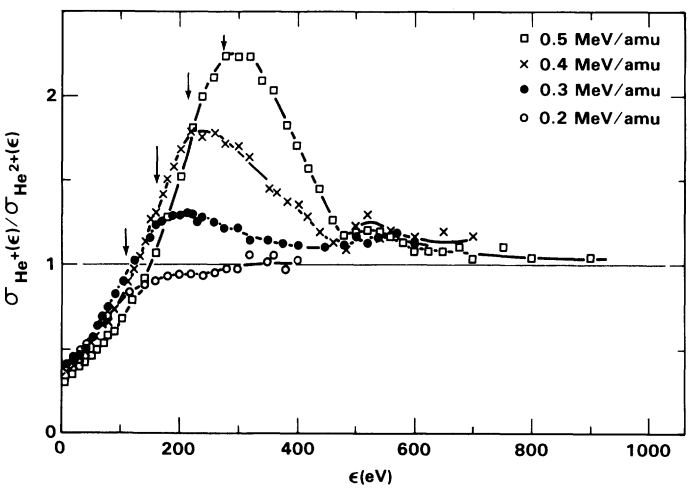

FIG. 6. Ratio of single differential cross sections for ionization of water vapor by He^+ to those for He^{2+} plotted vs the ejected electron energy. The arrows indicate the energy at which the incident ion and ejected electron velocities are equal in magnitude.

energy of the stripped electron peak is somewhat higher than one would expect if the electron were ejected with zero energy in the rest frame of the moving ion. The arrows shown in Fig. 6 indicate the expected peak centroid energy corresponding to $v_e = v_i$ for the respective ion energies. The measured peak energy is about 25 eV higher at each ion energy than expected. This shift in peak energy does not appear to be an artifact of screening which conceivably could change the apparent peak position by suppressing the ratio on the low-energy side of the peak. This will be discussed further in the next paragraph. It is also unlikely that the peak energy is shifted to higher energy due to a concentration of excited He^+ ions in the primary beam. Such states would have to be very long lived since the transit time from production to target is more than 0.5 μsec for the fastest ions and quenching of metastable states should occur as the beam passes through the analyzing and inflection magnets.

Analyses of the ratios of Fig. 6 provide an opportunity to derive a screening function which represents the degree to which the He^+ nucleus is screened by the bound electron as a function of the energy loss by the incident ion ($E = \epsilon + I$). If we define the screening function $S(\epsilon)$ such that

$$Z_{\text{eff}} = S(\epsilon) Z, \tag{3}$$

where Z_{eff} is the effective nuclear charge and Z the bare ion charge, then $\sigma(\epsilon)$ is proportional to $S^2(\epsilon)Z^2$ and $S(\epsilon)$ can be obtained from the measured cross sections by the expression:

$$S(\epsilon) = [\sigma_{He^{2+}}(\epsilon)/\sigma_{He^+}(\epsilon)]^{1/2}. \tag{4}$$

The screening function derived from these data in this way is shown in Fig. 7 along with cross section ratios recalculated including a screening "correction" for the

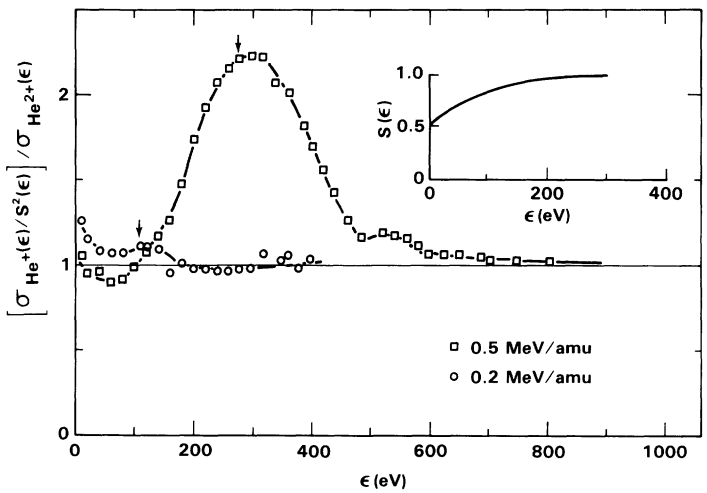

FIG. 7. Ratio of the single differential cross sections for He^+ corrected as described in the text for screening of the nuclear charge by the bound electron to the equivalent velocity He^{2+} cross sections. The screening function $S(\epsilon)$ is plotted vs ejected electron energy in the inset. The arrows indicate the energy at which the ejected electron and incident ion velocities are equal in magnitude.

He^+ data. This correction removes, to a first approximation, the influence of screening on the shape of the electron loss peak. Note that this correction has little, if any, effect on the centroid energy of the electron loss peak. Although there is some ion energy dependence, as was discussed earlier for the double differential cross sections, a simple screening function is sufficient to reduce the ratio:

$$R = [\sigma_{He^+}(\epsilon)/S^2(\epsilon)Z^2]/[\sigma_{He^{2+}}(\epsilon)/Z^2] \quad (5)$$

to a value of 1 to within about ±15% for all ion energies in the present study, except, of course, in the electron energy region where electron stripping dominates.

The structure at the high-energy edges of the stripped electron peak visible in Figs. 7 and 8 is due to the presence of Auger electron emission in the electron spectra (*29*). Because of the small impact parameters associated with inner shell ionization, one would expect He^+ and He^{2+} to be equally effective in production of inner shell vacancies in the water vapor molecule. Adding a constant Auger intensity to each spectrum will cause the ratio to tend toward a value of 1 in the energy region of Auger emission spectrum. This is observed as a dip in the ratio at about 500 eV.

The application of Z^2 scaling for single differential cross sections for electron emission can be examined by analysis of ratios of cross sections for He^{2+} and protons. Such ratios are shown in Fig. 8 for ion energies of 0.3 and 0.5 MeV/amu. The ratio is within ±20% of unity, the value expected for Z^2 scaling. For ejected electron energies above about 500 eV, the ratio is 1 within the 10% precision of the measurement as illustrated by the error bar shown in Fig. 8. For ejected electron energies below 500 eV, although the variation is small, the ratio varies systematically from a value of 1. The increase in the ratio above 1 in the energy range from about 100 to 500 eV may be attributed to the effects of continuum-charge-transfer.

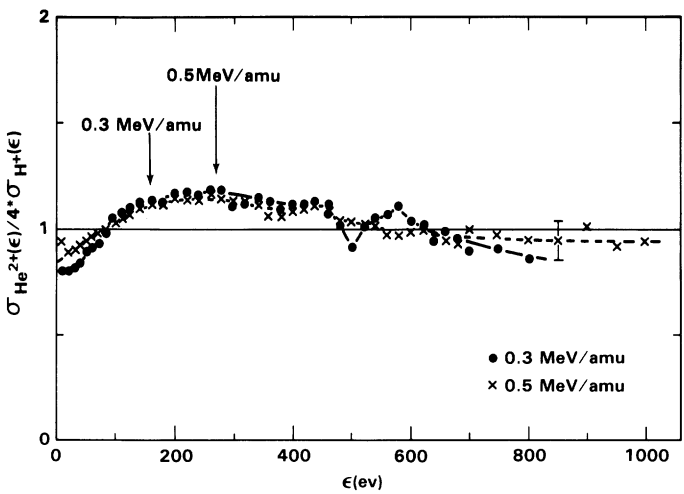

FIG. 8. Ratio of single differential electron emission cross sections for equal velocity protons and He^{2+} ions (α particles). The proton data from Ref. (*7*) have been multiplied by 4 for Z^2 scaling. The arrows indicate the energy at which the ejected electron and incident ion velocities are equal in magnitude.

This process is expected to occur for electron energies near $v_i = v_e$ (the arrows indicate this equal velocity condition in Fig. 8) and to scale with higher powers of ion charge than Z^2 (*27, 28*). Unfortunately, we have no way to separate accurately charge transfer electrons from direct ionization electrons, and therefore we cannot determine the charge scaling dependence of these ionization mechanisms independently.

For low-energy electron ejection, the ratio of He^{2+} cross sections to Z^2 scaled proton results is less than one. We have no explanation for this behavior. It is certainly an unexpected result if Z^3 contributions derived from stopping power theory are used as a guide (*30*). Such calculations predict an enhancement of this ratio for very small values of energy loss. Although experimental difficulties make our cross section measurements for electron energies less than about 15 eV unreliable, we have no reason to question the reliability of cross sections for higher energy electrons, and the ratios shown in Fig. 8 are systematically and significantly below 1 at energies as high as 25 eV.

TOTAL IONIZATION AND PARTIAL STOPPING CROSS SECTIONS

The total ionization cross section and partial stopping cross sections can be obtained by integration of the measured double differential cross sections. The total ionization cross section is obtained from:

$$\sigma_T = 2\pi \int_0^{\epsilon_{max}} \int_{-1}^{-1} \sigma(\epsilon,\theta) d\epsilon d(\cos\theta). \tag{6}$$

This procedure assumes the emission cross sections are independent of the azimuthal angle ϕ so that the integration over solid angle can be simplified to the form applied in Eq. (6). For the charged particle velocity range of the present measurements, the major contribution to stopping power results from ionization (*1, 2*). Energy lost as kinetic energy of the ejected electrons and energy lost in overcoming the binding energy of the ejected electrons account for as much as 90% of the stopping power of 0.5 MeV/amu ions (*1*). The partial stopping power for ionization, S_I, can be obtained from our measurements by the following relationship:

$$S_I = I \int \sigma(\epsilon,\theta) d\epsilon d\Omega + \int \epsilon\sigma(\epsilon,\theta) d\epsilon d\Omega, \tag{7}$$

where I is the binding energy of the ejected electron and $d\Omega$ is the differential solid angle (*2*). Because of the importance of the spatial distribution of absorbed energy in radiation damage, a quantity of interest to radiation physics is the mean kinetic energy of the ejected secondary electrons. The mean energy can be determined from

$$\bar{\epsilon} = \int \epsilon\sigma(\epsilon,\theta) d\epsilon d\Omega \Big/ \int \sigma(\epsilon,\theta) d\epsilon d\Omega. \tag{8}$$

A compilation of the total ionization cross section, σ_T, mean electron energy, $\bar{\epsilon}$, and partial stopping power for energy loss to kinetic energy of secondary electrons,

TABLE I

Mean Electron Energies, Total Ionization, and Partial Stopping Cross Sections

Ion energy (MeV/amu)	He^{2+}			He^{+}			H^{+}		
	σ_T[a]	$\bar{\epsilon}$[b]	$\bar{\epsilon}\sigma_T$[c]	σ_T	$\bar{\epsilon}$	$\bar{\epsilon}\sigma_T$	σ_T	$\bar{\epsilon}$	$\bar{\epsilon}\sigma_T$
0.075	1.23			0.838	39	33.0			
0.20	1.23	45	55.6	0.661	63	41.6			
0.30	0.90	52	47.1	0.557	78	43.3	0.257	45	11.6
0.40	0.95	49	46.7	0.476	92	44.1			
0.50	0.77	51	39.5	0.362	112	40.5	0.170	56	9.6

[a] σ_T in units of 10^{-15} cm^2.
[b] $\bar{\epsilon}$ in units of eV.
[c] $\bar{\epsilon}\sigma_T$ in units of 10^{-15} eVcm^2.

$\bar{\epsilon}\sigma_T$, is shown in Table I. The mean electron energy for ionization by equal velocity He^{2+} and H^+ is the same to within about 10%. Such agreement is also observed between the total ionization cross section for He^{2+} and the proton cross section multiplied by a factor of 4 to account for Z^2 scaling. The mean energy of electrons resulting from He^+ collisions is, however, considerably larger than those from bare ion collisions. The mean ejected electron energy for He^+ ions increases rapidly with velocity in contrast to the nearly constant value for the bare projectiles. The mean electron energy increases by more than a factor of 2 for ion energies going from 0.075 to 0.5 MeV/amu. The total electron yield (i.e., total ionization cross section) for He^{2+} impact is from 1.8 to 2 times greater than the corresponding He^+ value throughout the range of particle energies studied here. This would imply that the He^+ ion can be assigned an effective charge of about 1.4 with regard to total electron production, which is somewhat larger than the value 1.2 determined for numerous other target molecules by Pucket *et al.* (*31*). It should be emphasized that the concept of an effective charge has meaning only for total cross sections since we have shown the effective nuclear charge is a function of energy loss for differential ionization cross sections due to screening. It is interesting to note that, although the ionization cross sections and mean ejected electron energies are quite different for He^+ and He^{2+} collisions, the product of these quantities, which is the partial stopping cross section for transfer of energy to secondary electrons, is nearly equal for the two ions.

As indicated above, the partial stopping power for ionization is the sum of energy loss to overcome the ejected electron's binding energy and the kinetic energy imparted to that electron. This quantity was calculated from our data using Eq. (7) assuming that all ejected electrons were valence bound. These results are compared to recent total stopping cross section measurements for water vapor (*32, 33*) in Table II. The partial cross sections are somewhat larger for He^{2+} than He^+, and a charge-state weighted average must be used for comparison to measured stopping cross sections since those measurements include equilibrium charge states for the helium ion beam. The equilibrium charge states were estimated from the data presented for helium ions in air by Allison (*34*) and charge-state averaged partial

TABLE II

Partial and Total Stopping Cross Sections

	Partial stopping cross section[a]			*Stopping cross sections*[b]	
Ion energy (MeV/amu)	He^+	He^{2+}	*Charge state average*	*Matteson* et al.[c]	*Palmer and Akhavan-Rezayat*[d]
0.075	43.5			63.2	
0.200	50	71	60.5	72.9	86
0.300	50	58	56	66.6	64
0.400	50	59	58	58.7	56
0.500	45	49	49	52.1	50.8

[a] Partial stopping cross section including contributions from binding energy and kinetic energy of electrons released in ionizing collisions; cross sections in units of 10^{-15} eV·cm²/molecule.

[b] Stopping cross section in units of 10^{-15} eV cm²/molecule.

[c] See Ref. (*32*).

[d] See Ref. (*33*).

stopping cross sections were calculated. These are tabulated in Table II. Although the major contribution to stopping power in this energy range is ionization, we would expect our values to be smaller than the total cross sections with the difference attributed primarily to energy loss through excitation of the target molecule. Our partial cross sections are smaller than the total cross sections of Matteson *et al.* (*32*) by about 20% at 0.2 MeV/amu and 5–10% at the higher energies. These differences are in agreement with the expected contributions for excitation in this energy range presented by Miller and Green (*1*) in their discussion of stopping power for fast protons. Our results are more nearly in agreement with the measurements of Palmer and Akhavan-Rezayat (*33*) with the exception of the 0.2 MeV/amu point where their value is considerably larger than the results of Matteson *et al.* The agreement between our data and Palmer and Akhavan-Rezayat would imply a smaller contribution due to excitation than the comparison with the work of Matteson *et al.* Because these differences are within the absolute uncertainties in the measurements, the primary conclusion to be drawn from this comparison is that the differential cross sections, which provide considerable detail with regard to the kinematics of energy deposition, also provide partial stopping cross sections in good agreement with cross sections derived in an entirely different manner. This agreement reinforces our confidence in the accuracy of the differential cross sections, which are subject to numerous experimental uncertainties not inherent in total cross section measurements, and provides insight into the stochastics of the energy-loss process leading to the stopping of charged particles in matter.

CONCLUSIONS

Cross sections, differential in ejected electron energy and emission angle and measured for 0.075 to 0.5 MeV/amu helium ions, clearly demonstrate the importance of projectile structure in the ionization of water vapor. The bound electron associated with the He^+ ion acts effectively to screen the nuclear charge at large

impact parameters and produces a sizable contribution to the ejected electron spectra as it is stripped from the incident ion. These effects lead to electron spectra of higher mean energy and lower total yield for He^+ than the bare He^{2+} ion. The partial stopping power for ionization also differs for He^+ and He^{2+} but to a much lesser degree.

Comparison of the cross sections for He^{2+} impact with previous measurements for protons indicate that deviations from Z^2 scaling occur primarily for electron emission into small angles and for electron velocities similar to the ion velocity. These disparities are attributed to contributions to the electron spectra from the continuum-charge-transfer process, which has been shown to have a higher order dependence on Z than Z^2. In addition, Z^2 scaling appears to fail for low-energy electron ejection, $\epsilon \lesssim 75$ eV, where the yield from He^{2+} ions is somewhat smaller than expected based on Z^2 scaling of proton data. The disparity is in the opposite direction from the predictions of Z^3 contributions to stopping power, and we can offer no explanation for this behavior at this time.

RECEIVED: October 19, 1979; REVISED: December 13, 1979

REFERENCES

1. J. H. MILLER and A. E. S. GREEN, Proton energy degradation in water vapor. *Radiat. Res.* **54,** 343–363 (1973).
2. W. E. WILSON, Stopping power partition and mean energy loss for energetic protons in hydrogen. *Radiat. Res.* **49,** 36–50 (1972).
3. M. E. RUDD and J. H. MACEK, Mechanisms of electron production in ion-atom collisions. *Case Stud. At. Phys.* **3,** 47–136 (1972).
4. S. T. MANSON, L. H. TOBUREN, D. H. MADISON, and N. STOLTERFOHT, Energy and angular distribution of electrons ejected from helium by fast protons and electrons: Theory and experiment. *Phys. Rev. A* **12,** 60–79 (1975). [And references therein.]
5. W. E. WILSON and L. H. TOBUREN, Electron emission from proton-hydrocarbon-molecule collisions at 0.3–2.0 MeV. *Phys. Rev. A* **11,** 1303–1308 (1975).
6. D. J. LYNCH, L. H. TOBUREN, and W. E. WILSON, Electron emission from methane, ammonia, monomethylamine, and dimethylamine by 0.25 to 2.0 MeV protons. *J. Chem. Phys.* **64,** 2616–2622 (1976).
7. L. H. TOBUREN and W. E. WILSON, Energy and angular distributions of electrons ejected from water vapor by 0.3–1.5 MeV protons. *J. Chem. Phys.* **66,** 5202–5213 (1977).
8. L. H. TOBUREN, W. E. WILSON, and L. E. PORTER, Energy and angular distributions of electrons ejected from the ionization of SF_6 and TeF_6 by fast protons. *J. Chem. Phys.* **67,** 4212–4221 (1977).
9. T. L. CRISWELL, L. H. TOBUREN, and M. E. RUDD, Energy and angular distribution of electrons ejected from argon by 5-keV to 1.5-MeV protons. *Phys. Rev. A* **16,** 508–517 (1977).
10. L. H. TOBUREN, S. T. MANSON, and Y.-K. KIM, Energy distributions of secondary electrons. III. Projectile energy dependence for ionization of He, Ne, and Ar by protons. *Phys. Rev. A* **17,** 148–159 (1978).
11. M. E. RUDD and D. H. MADISON, Comparison of experimental and theoretical electron ejection cross sections in helium by proton impact from 5 to 100 keV. *Phys. Rev. A* **14,** 128–136 (1976).
12. M. E. RUDD, Mechanisms of electron production in ion-atom collisions. *Radiat. Res.* **64,** 153–180 (1975).
13. L. H. TOBUREN, Distribution in energy and angle of electrons ejected from molecular nitrogen by 0.3–1.7 MeV protons. *Phys. Rev. A* **3,** 216–228 (1971).
14. M. E. RUDD and R. D. DUBOIS, Absolute doubly differential cross sections for ejection of secondary electrons from gases by electron impact. I. 100- and 200-eV electrons on helium. *Phys. Rev. A* **16,** 26–32 (1977).

15. R. D. DuBois and M. E. Rudd, Absolute double differential cross sections for ejection of secondary electrons from gases by electron impact. II. 100–500 eV electrons on neon, argon, molecular hydrogen, and molecular nitrogen. *Phys. Rev. A* **17,** 843–848 (1978).

16. N. Oda, F. Nishimura, and S. Tahira, Energy and angular distributions of secondary electrons resulting from ionizing collisions of electrons with helium and krypton. *J. Phys. Soc. (Jpn.)* **33,** 462–467 (1972).

17. E. C. Beaty, K. H. Hesselbacker, S. P. Hong, and J. H. Moore, Measurements of the triple-differential cross sections for low-energy electron-impact ionization of helium. *Phys. Rev. A* **17,** 1592–1599 (1978). [And references therein.]

18. S. P. Hong and E. C. Beaty, Measurements of the triple-differential cross section for low-energy electron-impact ionization of argon. *Phys. Rev. A* **17,** 1829–1836 (1978).

19. C. B. Opal, W. K. Peterson, and E. C. Beaty, Measurements of secondary-electron spectra produced by electron impact ionization of a number of simple gases. *J. Chem. Phys.* **55,** 4100–4106 (1971).

20. C. B. Opal, E. C. Beaty, and W. K. Peterson, Tables of secondary electron production cross sections. *Atomic Data* **4,** 209–253 (1972).

21. M. E. Rudd, T. Jorgensen, Jr., and D. J. Volz, Electron energy spectrum from Ar^+-Ar and H^+-Ar collisions. *Phys. Rev.* **151,** 28–31 (1977).

22. R. K. Cacak and T. Jorgenson, Jr., Absolute double differential cross sections for production of electrons in Ne^+-Ne and Ar^+-Ar collisions. *Phys. Rev. A* **2,** 1322–1327 (1970).

23. N. Stolterfoht, D. Schneider, D. Burch, H. Wieman, and J. S. Risley, Mechanisms for electron production in 30 MeV O^{n+} + O_2 collisions. *Phys. Rev. Lett.* **33,** 59–62 (1974).

24. L. H. Toburen and W. E. Wilson, Differential cross sections for ionization of argon by 0.3–2.0 MeV He^{2+} and He^+ ions. *Phys. Rev. A* **19,** 2214–2224 (1979).

25. L. H. Toburen, Differential cross sections for electron emission in heavy ion collisions. *IEEE Trans. Nucl. Sci.* NS-**26,** 1056–1061 (1979).

26. M. Inokuti, Inelastic collisions of fast charged particles with atoms and molecules—The Bethe theory revisited. *Rev. Mod. Phys.* **43,** 297–347 (1971).

27. C. R. Vane, I. A. Sellin, M. Suter, G. D. Alton, S. B. Elston, P. M. Griffin, and R. S. Thoe, Z, velocity, and charge dependence of zero-degree electron 'cusps' from charged transfer to continuum states of bare and highly ionized projectiles. *Phys. Rev. Lett.* **40,** 1020–1023 (1978).

28. K. Dettman, K. G. Harrison, and M. W. Lucas, Charge exchange to the continuum for light ions in solids. *J. Phys. B* **7,** 269–287 (1974).

29. L. H. Toburen, K-shell ionization by fast protons. In *Proceedings of the International Conference on Inner Shell Phenomena and Future Applications* (R. W. Fink, S. T. Manson, J. M. Palms, and P. V. Rao, Eds.), Vol. 2, pp. 979–992, 1972. [Available as CONF-720404 from National Technical Information Service, Springfield, VA 22161.]

30. J. H. Miller, Z^3 effect in the ionization cross section of argon by 1.2- and 2.0-MeV alpha particles. *Phys. Rev. A* **16,** 2478–2479 (1977).

31. L. J. Puckett, G. O. Taylor, and D. W. Martin, Cross sections for ion and electron production in gases by 0.15–1.00 MeV hydrogen and helium ions and atoms. *Phys. Rev.* **178,** 271–287 (1969).

32. S. Matteson, D. Power, and E. K. L. Chau, Physical-state effect in the stopping cross section of H_2O ice and vapor for 0.3–2.0 MeV alpha particles. *Phys. Rev. A* **15,** 856–864 (1977).

33. R. B. J. Palmer and A. Akhavan-Rezayat, Range-energy relation in stopping power of water, water vapor, and tissue-equivalent liquids for alpha particles over the energy range 0.5 to 8 MeV. In *Proceedings of the Sixth Symposium on Microdosimetry* (J. Booz and H. G. Ebert, Eds.), pp. 739–748. Harwood, Amsterdam, 1978.

34. S. K. Allison, Experimental results on charge-changing collisions of hydrogen and helium ions and atoms at kinetic energies above 0.2 keV. *Rev. Mod. Phys.* **30,** 1137–1168 (1958).